To the Graduate Council:

I am submitting herewith a thesis written by John Darrek Offutt entitled "Crack-Face Interaction for a Griffith Crack in Biaxial Stress." I have examined the final copy of this thesis for form and content and recommend that it be accepted in partial fulfillment of the requirements for the degree of Master of Science, with a major in Engineering Science.

J. A. M. Boulet, Major Professor

We have read this thesis
and recommend its acceptance:

Accepted for the Council:

Vice Provost
and Dean of the Graduate School

STATEMENT OF PERMISSION TO USE

In presenting this thesis in partial fulfillment of the requirements for a Master's degree at The University of Tennessee, Knoxville, I agree that the Library shall make it available to borrowers under rules of the Library. Brief quotations from this thesis are allowable without special permission, provided that accurate acknowledgment of the source is made.

Permission for extensive quotation from or reproduction of this thesis may be granted by my major professor, or in his absence, by the Head of Interlibrary Services when, in the opinion of either, the proposed use of the material is for scholarly purposes. Any copying or use of the material in this thesis for financial gain shall not be allowed without my written permission.

Signature John Daniel Gibbs

Date August 17, 1989

CRACK–FACE INTERACTION FOR A GRIFFITH CRACK IN BIAXIAL STRESS

A Thesis

Presented for the

Master of Science

Degree

The University of Tennessee, Knoxville

John Darrek Offutt

December 1989

To Reneaue´

ACKNOWLEDGMENTS

The author wishes to express his gratitude to Dr. J.A.M. Boulet for his guidance and encouragement during the preparation of this thesis and thank Dr. T.G. Carley and Dr. J.D. Landes for their contibutions as committee members.

ABSTRACT

The work described herein is an investigation of the influence of crack-face interaction on unstable crack propagation in brittle materials. For this study, interaction results from the interference of wedge-shaped protrusions on the faces of a Griffith crack when subjected to arbitrarily oriented biaxial stress at infinity. A mathematical model based on solutions from linear elastic theory is presented for a single interference site and then expanded to include multiple interference sites. The importance of protrusion interference is measured as the change in the fracture toughness required to prevent unstable crack propagation in the presence of interference from that required in the absence of interference. The dependence of the required fracture toughness on the applied stress (orientation and magnitude), wedge geometry (size and vertex angle), and configuration of the interference sites (location and number) is examined, with all results obtained for dimensionless variables. It is concluded that a single interference site has little effect on the required fracture toughness, except under certain special conditions. For multiple sites, although the effect on the required fracture toughness increases monotonically with the number of sites, it appears to approach some limit asymptotically.

TABLE OF CONTENTS

CHAPTER		PAGE
1	INTRODUCTION	1
2	FORMULATION FOR A SINGLE INTERFERENCE SITE	3
	Interference Model	3
	Compatibility Condition	8
	Conditions for Interference to Occur	9
	Iteration Procedure	16
	Fracture Criterion	17
3	SOLUTION TO PROBLEM A	20
	Complex Variable Formulation	20
	Biaxial Stress at Infinity	22
	Concentrated Loads on the Crack Faces	25
	Load-Displacement Relationship	29
4	SOLUTION TO PROBLEM B	31
	Complex Variable Formulation	31
	Solution Method	32
	Load-Displacement Relationship	33
5	FORMULATION FOR MULTIPLE INTERFERENCE SITES	35
6	RESULTS AND CONCLUSIONS	39
	Results for a Single Interference Site	39
	Results for Multiple Interference Sites	46
	Conclusions	50
	LIST OF REFERENCES	51
	VITA	53

LIST OF TABLES

TABLE		PAGE
2.1	Restrictions on the Biaxial Stress Ratio	11
2.2	Biaxial Stress Cases	11
2.3	Intervals in Which the Biaxial Stress Ratio is Unrestricted	14

LIST OF FIGURES

FIGURE		PAGE
2.1	Interference Region	5
2.2	Representation of Problem A	5
2.3	Qualitative Representation of Wedge Bending	6
2.4	Representation of Problem B	6
2.5	Relationship Between the Concentrated Loads in Problem A and the Contact Force in Problem B	7
2.6	Regions in Which the Various Cases of Biaxial Stress Produce Interference	12
2.7	Dependence of the Boundary Between Biaxial Stress Cases I and IV on the Wedge Half-Angle, α	15
3.1	Infinite Plate With a Central Crack	26
6.1	Dependence of the Required Fracture Toughness Ratio on the Wedge Half-Angle, α	40
6.2	Dependence of the Required Fracture Toughness Ratio on the Stress Orientation Angle, β	42
6.3	Dependence of the Required Fracture Toughness Ratio on the Biaxial Stress Ratio, ρ	43
6.4	Dependence of the Required Fracture Toughness Ratio on Poisson's Ratio, ν	44
6.5	Dependence of the Required Fracture Toughness Ratio on the Wedge Height	45
6.6	Dependence of the Required Fracture Toughness Ratio on the Location of the Interference Site	47
6.7	Dependence of the Required Fracture Toughness Ratio on the Number of Interference Sites	48
6.8	Illustration of the Required Fracture Toughness Ratio Approaching a Limit Asymptotically as the Number of Interference Sites is Increased	49

1

INTRODUCTION

In the theory of linear elastic fracture mechanics, the stress intensity factors provide a measure of the crack tip stress field. For a crack subjected to a general loading, these stress intensity factors may be combined by means of a fracture criterion to estimate the fracture toughness required to prevent unstable crack propagation. In general, the analysis of a cracked body does not involve considerations for interaction of the crack faces. Nevertheless, various types of crack-face interaction are possible in real cracks. For compressive stresses, closure of the crack can bring the faces into contact. For biaxial tension with the crack inclined to both principal stresses, interference between the protrusions on rough faces can occur. Furthermore, interaction can take place in fibrous composites when fibers which bridge the crack are present. Any crack-face interaction will affect the crack tip stress field, and so change the stress intensity factors from what they would be if the interaction were not present. As a result, the estimate of the required fracture toughness is changed. The extent to which this value changes is a direct indication of the importance of the interaction.

In the classical analysis of a Griffith crack subjected to arbitrarily oriented biaxial stress at infinity [1], the crack faces do not interact. Under biaxial stress, the crack tends to open or close depending on the orientation and signs of the applied stresses. In addition, if the crack is not aligned with either principal direction, the stresses tend to shear the crack. Since the faces of real cracks typically have irregular geometries, shearing can cause the protrusions on opposing faces to interfere with each other. Consequently, forces are produced which will influence the crack tip stress field.

The specific type of crack-face interaction examined herein is that of protrusion interference resulting from relative shear displacement of the crack faces. In this analysis, we consider a Griffith crack with protrusions on the crack faces and arbitrarily oriented biaxial stress at infinity. Our objective is to evaluate the effects of protrusion interference on the initiation of fracture in a brittle material.

2

FORMULATION FOR A SINGLE INTERFERENCE SITE

For our initial investigation, we assume the crack to be opened such that protrusion interference occurs at only one location and that the region in which the interference takes place is small compared to the crack size. In order to assess the importance of this type of crack-face interaction, the forces it generates must first be determined. Hence, a model of the interference is required.

Interference Model

The interference model was proposed by Dr. J.A.M. Boulet, Associate Professor of Engineering Science and Mechanics at the University of Tennessee, Knoxville, and requires solutions for two elasticity problems. In these problems, referred to hereinafter as problems A and B, concentrated loads are used to represent the forces produced by interference. Problem A is a Griffith crack subjected to arbitrarily oriented biaxial stress at infinity and concentrated loads on the crack faces. Problem B is a half-plane with an interference site on the boundary subjected to concentrated loads statically equivalent to those used in problem A. From the solution to each problem, the relative displacement of the crack faces can be obtained. The interference forces are then found with an iteration procedure based on compatibility of displacements for problems A and B in the linear theory of elasticity. (The assumption of linearity is appropriate for the analysis of fracture in brittle materials.) The correct values of the interference forces are those for which problems A and B will have compatible relative displacements.

Our representation of the interference region is illustrated in Figure 2.1, where the protrusions are assumed to be wedge-shaped. While not realistic, the wedge geometry is more convenient, mathematically, than a rectangular or step geometry. Since we assume that the interference region is much smaller than the crack, the effect of interference on the crack tip stress field is the same as if the wedges were replaced with concentrated loads. Problem A is then represented by Figure 2.2, where the interaction site is located at $x = b$.

When the wedges are brought into contact they deform elastically, as illustrated quantitatively in Figure 2.3. Since the deformation is essentially bending, contact occurs over a finite region, the contact patch, which is assumed to be small compared to the other dimensions of the wedge. Although the pressure on the contact patch is generally not uniform, our analysis is greatly simplified if we assume this patch to be a point. Consequently, the pressure distributed over the contact patch can be replaced with a concentrated force. The difference in the stress field of this simpler problem will be confined to the vicinity of the point where the concentrated force is applied. Since our interest is in the stress field at the crack tip, the deviation at the wedge is not important for this investigation. Thus, as shown in Figure 2.4, problem B is that of a half-plane with a wedge-shaped protrusion on the boundary subjected to a concentrated force applied normal to the face of the wedge.

In order to relate the concentrated load in problem B to those in problem A, we consider the stresses produced along the base of the wedge by the contact force, P, shown in Figure 2.4. Far from the wedge, the stresses will have the same effect as their statically equivalent concentrated loads. These concentrated loads, and their relationship to the contact force, P, are shown in Figure 2.5.

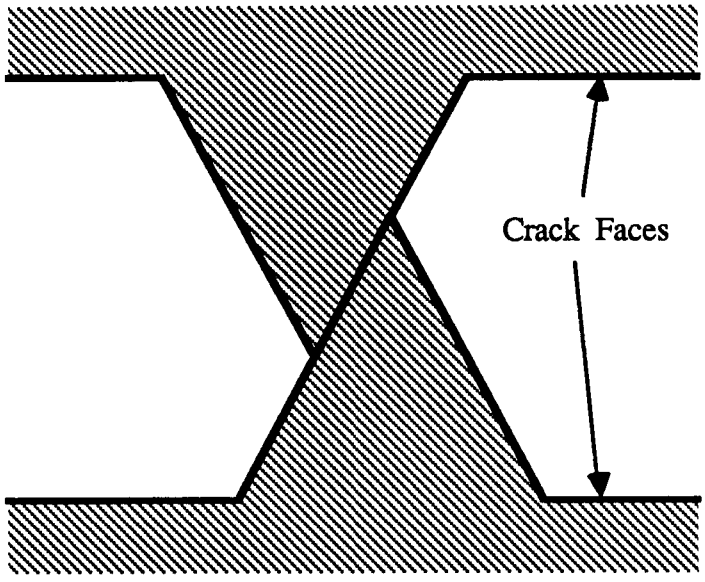


Figure 2.1. Interference Region. Interference between wedge-shaped protrusions on the faces of a Griffith crack is represented.

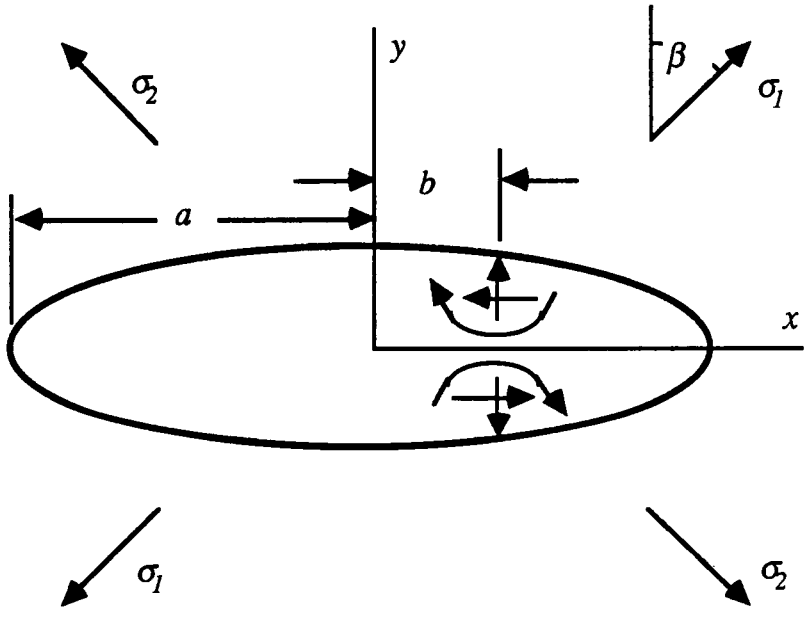


Figure 2.2. Representation of Problem A. A Griffith crack subjected to arbitrarily oriented biaxial stress at infinity and concentrated loads on the crack faces. The interference site is located at $x = b$.

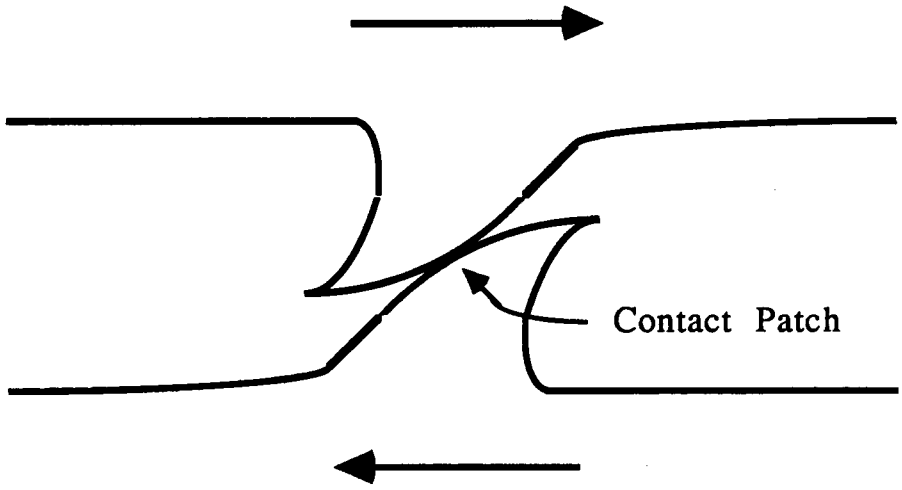


Figure 2.3. Qualitative Representation of Wedge Bending. Exaggerated bending of the wedge-shaped protrusions resulting from relative shear displacement of the crack faces.

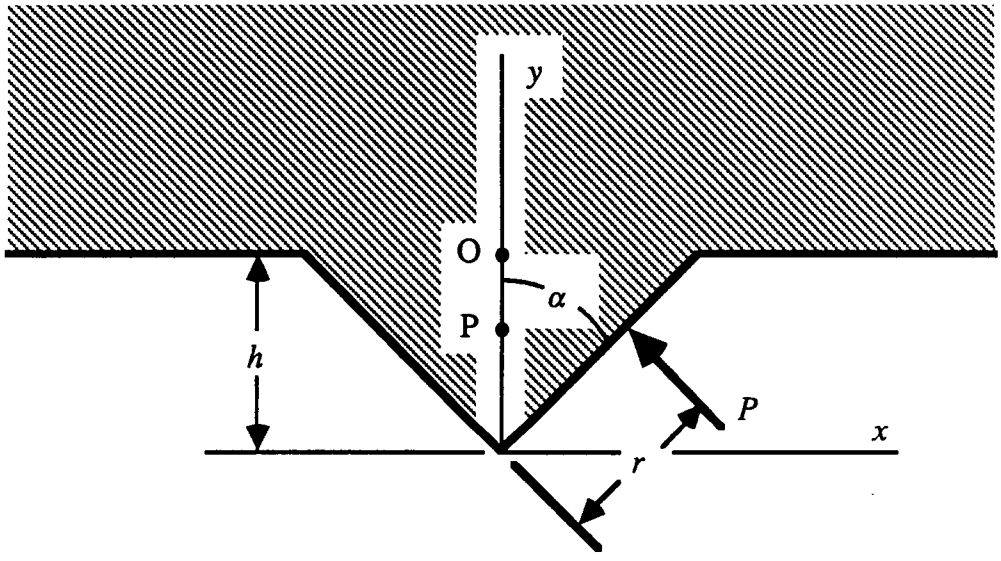


Figure 2.4. Representation of Problem B. A half-plane with a wedge-shaped protrusion on the boundary subjected to a concentrated force applied normal to one face of the wedge.

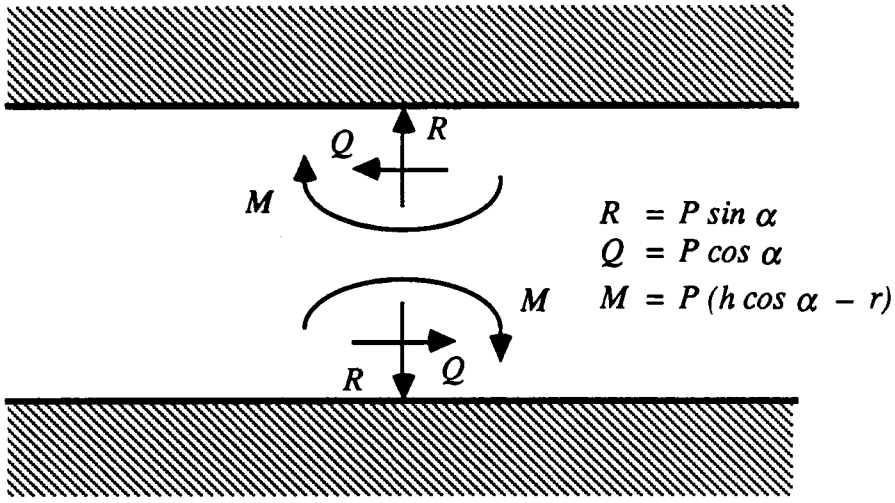


Figure 2.5. Relationship Between the Concentrated Loads in Problem A and the Contact Force in Problem B. The concentrated loads shown are statically equivalent to the stresses on the line $y = h$ in Figure 2.4 where $|x| < h \tan \alpha$.

Compatibility Condition

Earlier, the correct value of the contact force was identified as being the one which gave compatible displacements for problems A and B. Before this value can be found though, the compatibility condition must be established precisely. Let us define displacements u and v in the x and y directions, respectively (Figures 2.2 and 2.4). For the protrusion geometry selected, the relative displacements of Problems A and B must conform to the wedge bending shown in Figure 2.3. In problem A, the displacements of the upper crack face relative to those of the lower crack face are

$$\Delta u = (u^+)_{y=0} - (u^-)_{y=0} \tag{2.1}$$

$$\Delta v = (v^+)_{y=0} - (v^-)_{y=0} \tag{2.2}$$

Consequently, the wedge bending displacement for this problem can be written as (see Figures 2.1 and 2.4)

$$\delta_A = \Delta u - \Delta v \tan \alpha \tag{2.3}$$

where α is the wedge half-angle. Since the wedges in problem A have been replaced with concentrated loads, we need to evaluate (2.3) near where the loads act. A convenient location for this is

$$x = b + h \tan \alpha \tag{2.4}$$

where b is the location of the wedges, and h is their height. This location corresponds to the point where the face of the wedge meets that of the crack and is as close as possible to the wedges without being inside them. (It would not be correct to evaluate δ_A at the point underneath where the concentrated loads act.) In problem B (Figure 2.4), the wedge bending can be expressed as the centerline x-direction displacement at the base of the wedge (point O) relative to that at the y coordinate of the contact force (point P).

But, problem A contains a pair of wedges, and so this expression must be multiplied by a factor of two in order to give values which are comparable to those of (2.3). Hence, the appropriate wedge bending displacement for problem B is

$$\delta_B = 2\,(u_O - u_P) \tag{2.5}$$

We now define the normalized contact force as

$$P^* = \frac{P}{\mu a} \tag{2.6}$$

where a is the crack half-length, and μ is the shear modulus. If the displacements of Problems A and B are to be compatible, P^* must be such that at the wedges

$$\delta_A^* = \delta_B^* \tag{2.7}$$

where the asterisk indicates dimensionless displacements which are normalized with respect to the crack half-length.

To impose the compatibility condition of (2.7), we first need to relate the contact load, P^*, to the relative displacements of problems A and B. The solutions to these problems are discussed in Chapters 3 and 4, respectively. And, since the load-displacement relationships are derived from these solutions, they too are presented in these chapters.

Conditions for Interference to Occur

For a given wedge pair, interference will take place only if certain physical conditions are satisfied. In general, these conditions limit the orientation and magnitude of the applied stresses. With the load-displacement relationship for problem A, which is identified as equation (3.39) at the end of Chapter 3, the restrictions imposed by these conditions can be expressed quantitatively.

One condition is that the relative shear displacement of the crack faces must be such that the wedges move toward, and not away from, each other. This requires that the applied stresses cause δ_A from (2.3) to be a positive quantity, for which Δu must necessarily exceed $\Delta v \tan \alpha$. We define the normalized applied stress as

$$\sigma^* = \frac{\sigma_1}{\mu} \tag{2.8}$$

and the biaxial stress ratio as

$$\rho = \frac{\sigma_2}{\sigma_1} \tag{2.9}$$

where σ_1 and σ_2 are the principal stresses shown in Figure 2.2. From the load-displacement relationship for problem A, equation (3.39), the preceding condition gives $A_1 > 0$. Since the contact load is not a factor in determining whether or not the applied stresses bring the wedges into contact, we set P^* to zero. Examination of (3.39) then leads to the restrictions in Table 2.1 where

$$\phi = \frac{\tan(\beta - \alpha)}{\tan \beta} \tag{2.10}$$

and β is the stress orientation angle (Figure 2.2). Unless these restrictions are satisfied, the applied stresses will not cause interference between the wedges.

Overall, biaxial stress admits four possible combinations of tensile and compressive principal stress. These combinations are labeled as cases I through IV in Table 2.2. Based on (2.10) and Tables 2.1 and 2.2, the conditions of β and ρ for which the various cases will produce interference are indicated in Figure 2.6. Note that for all but case I, there

Table 2.1. Restrictions on the Biaxial Stress Ratio. Unless these are satisfied, the wedges will not come into contact and interference will not occur. The quantity ϕ is defined in (2.10).

$\beta = \alpha - \frac{\pi}{2}$	$\sigma_1 > 0$	$\sigma_1 < 0$
$0 \le \beta \le 90^o$	$\rho < \phi$	$\rho > \phi$
$\beta^* < \beta < 0$	$\rho > \phi$	$\rho < \phi$
$-90^o \le \beta \le \beta^*$	$\rho < \phi$	$\rho > \phi$

Table 2.2. Biaxial Stress Cases. Labels for the four possible combinations of tensile and compressive principle stress are given in the rightmost column.

σ_1	σ_2	ρ	Case
> 0	≥ 0	≥ 0	I
> 0	≤ 0	≤ 0	II
< 0	≥ 0	≥ 0	III
< 0	≤ 0	≤ 0	IV

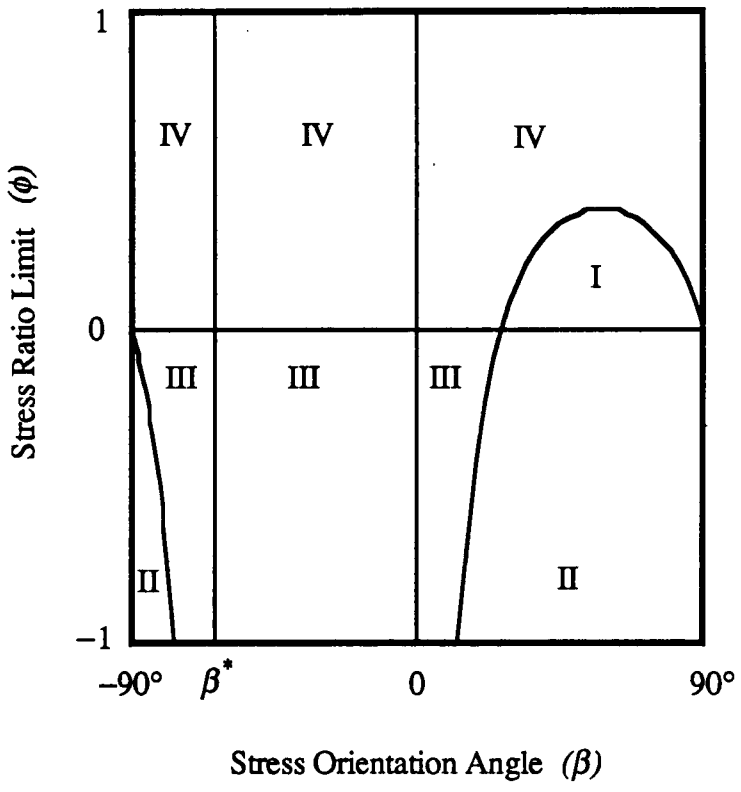


Figure 2.6. Regions in Which the Various Cases of Biaxial Stress Produce Interference. The curved lines indicate the quantity ϕ defined in (2.10). The lines $\beta = 0$ and $\beta = \beta^*$ are asymptotes (β^* is defined in Table 2.1, above). Between these lines, $\phi > 1$.

are intervals of the stress orientation angle, β, for which every value of ρ will produce interference. These intervals are given in Table 2.3.

For the value of the wedge half-angle, α, used in Figure 2.6, the probability of interference occurring for biaxial compression (case IV) is much greater than that for biaxial tension (case I). A measure of the probability that a particular stress case causes interference can be found as the ratio of the labeled area for that case to 2π, which is the total area defined by the values of β and ρ in Figure 2.6. The dependence of the regions corresponding to cases I and IV on α is illustrated in Figure 2.7 for $\rho > 0$. As the wedge half-angle is reduced, the probability of case IV causing interference decreases while that of case I increases.

Another condition which must be satisfied for interaction to occur is that the crack opening displacement must be small enough for the wedges to remain overlapped. This requires the opening displacement to be less than the wedge height, or

$$0 < \Delta v|_{x=b} < h \tag{2.11}$$

where the left-hand inequality prohibits interpenetration of the crack faces, and b is the location of the interaction site (Figure 2.2). In order for the right-hand inequality to be satisfied, the applied stresses must not be too large. For an interaction site located at $x = b$, the stress required to open the crack to a height $\Delta v = h$ at that site is

$$\sigma_h^* = \frac{2h}{(\kappa+1)(\cos^2\beta + \rho \sin^2\beta)\sqrt{a^2 - b^2}} \tag{2.12}$$

which follows from (3.39) with $P^* = 0$. For any given wedge, interference can only occur when $\sigma^* < \sigma_h^*$. In addition, for a given stress field and protrusion height, σ_h^* is a

Table 2.3. Intervals in Which the Biaxial Stress Ratio is Unrestricted. For these intervals of the stress orientaion angle, β, every value of the biaxial stress ratio, ρ, will produce interference.

Case	Interval
II	$\alpha < \beta < 90^o$
III	$\frac{-\pi}{2} + \frac{\alpha}{2} < \beta < \frac{\alpha}{2}$
IV	$-90^o < \beta < \alpha$

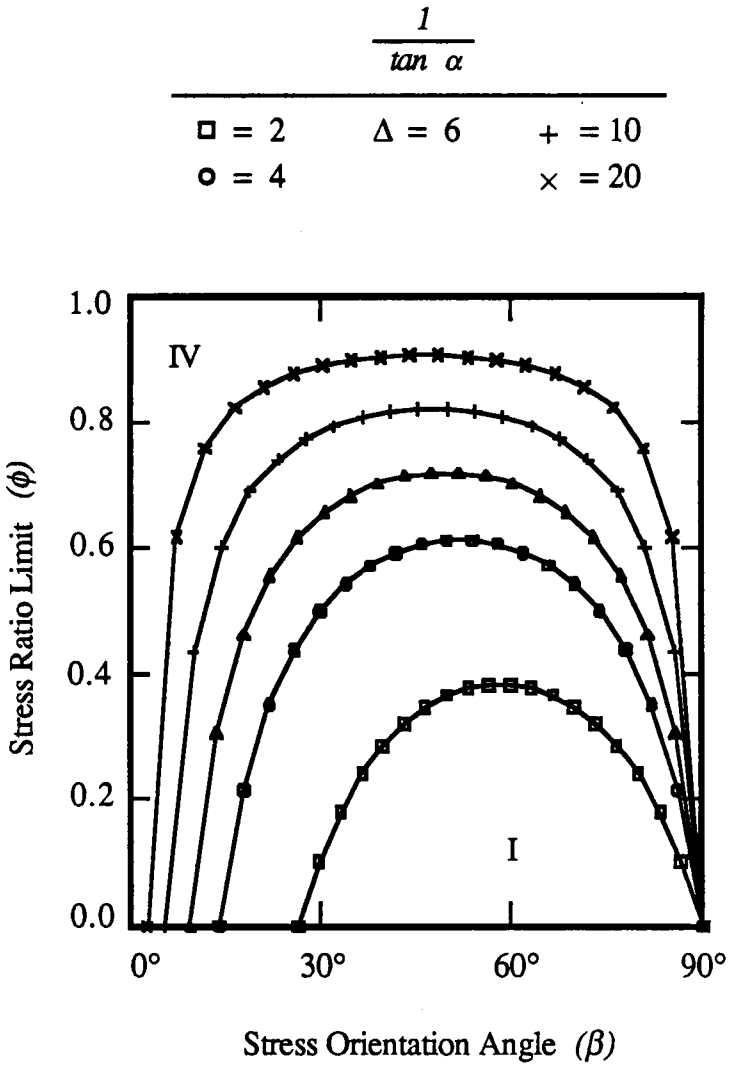


Figure 2.7. Dependence of the Boundary Between Biaxial Stress Cases I and IV on the Wedge Half-Angle, α. The curved lines are the quantity ϕ defined in (2.10) for the values of α shown. The region above a particular curve is case IV and the region below that curve is case I. As α decreases, the region in which case IV (biaxial compression) produces interference shrinks while that in which case I (biaxial tension) grows.

minimum when the wedge is located at the center of the crack ($b = 0$). Consequently, if the applied stress, σ^*, is such that

$$\sigma^* < \sigma_m{}^* \tag{2.13}$$

where

$$\sigma_m{}^* = \frac{2h}{(\kappa+1)(\cos^2\beta + \rho \sin^2\beta)\, a} \tag{2.14}$$

interference will occur at the center, and thus everywhere on the crack.

Although not a condition for interference, there are some physical restrictions on the magnitude of the contact load. The value of the contact load must satisfy the inequality

$$0 < P^* < \frac{A_1}{A_2} \tag{2.15}$$

where A_1 and A_2 are defined in (3.39). The left-hand inequality appears because the contact force is necessarily compressive, and the right-hand inequality prevents the value of the contact load from exceeding that which would be produced for a rigid wedge.

Iteration Procedure

To find the correct value of P^*, an iteration procedure based on the compatibility condition, (2.7), is used. First, an applied stress which satisfies (2.11) is chosen. Next, P^* is guessed within the limits of (2.15). The wedge bending displacement for problem A, $\delta_A{}^*$, can then be calculated from (3.39). Because of (2.7), this value of $\delta_A{}^*$ can be substituted into (4.8). A value of P^* for Problem B which corresponds to $\delta_A{}^*$ is then obtained. It can be easily shown that if a guessed value of P^* is higher/lower than the

correct value, the value of P^* from (4.8) will be lower/higher than the correct value. A bisection routine guided by this fact will converge rapidly to the correct value of P^*.

Fracture Criterion

Given the correct value of P^* from the iteration procedure, we need a fracture criterion to evaluate the effects of interaction on crack propagation. While several criteria are available for analyzing a crack subjected to mixed-mode loading, the Griffith energy criterion [2] is chosen for this initial investigation. Written in terms of stress intensity factors, this criterion is

$$K_I^2 + K_{II}^2 = K_{IC}^2 \tag{2.16}$$

where K_I is the mode I stress intensity factor, K_{II} is the mode II stress intensity factor and K_{IC} is the critical value of the mode I stress intensity factor. The dimensionless versions of these quantities are defined as

$$K_I^* = \frac{K_I}{\mu\sqrt{\pi a}}$$

$$K_{II}^* = \frac{K_{II}}{\mu\sqrt{\pi a}}$$

$$K_{IC}^* = \frac{K_{IC}}{\mu\sqrt{\pi a}}$$

When the contact force is present, we can derive the stress intensity factors for the right-hand crack tip ($x = a$) from results given in the literature [3]. They are

$$K_I^* = (K_I^*)_0(1 + \Delta_I) \tag{2.17}$$

$$K_{II}^* = (K_{II}^*)_0(1 - \Delta_{II}) \tag{2.18}$$

where

$$(K_I^*)_0 = D_I \sigma^*$$

$$(K_{II}^*)_0 = D_{II} \sigma^*$$

$$D_I = \cos^2 \beta + \rho \sin^2 \beta$$

$$D_{II} = (1 + \rho) \cos \beta \sin \beta$$

$$\Delta_I = \frac{\sin \alpha}{\pi D_I} \sqrt{\frac{1+B}{1-B}} \frac{P^*}{\sigma^*}$$

$$\Delta_{II} = \frac{\cos \alpha}{\pi D_{II}} \sqrt{\frac{1+B}{1-B}} \frac{P^*}{\sigma^*}$$

$$B = \frac{b}{a}$$

Substitution of these results into the fracture criterion, (2.16), gives

$$\sigma^* f(\sigma^*) = K_{IC}^* \tag{2.19}$$

where

$$f(\sigma^*) = \sqrt{\left[D_I(1 + \Delta_I)\right]^2 + \left[D_{II}(1 - \Delta_{II})\right]^2}$$

If interference is not present, this reduces to

$$\sigma_0^* f_0 = K_C^* \tag{2.20}$$

where

$$f_0 = \sqrt{D_I^2 + D_{II}^2}$$

If we assume that $\sigma^* = \sigma_0^*$ and that this value of the applied stress is the fracture stress, the significance of protrusion interference can be determined from (2.19) and (2.20) by

$$R = \frac{f_0}{f(\sigma^*)} \tag{2.21}$$

which is the ratio of the fracture toughness required in the absence of interference to that required in the presence of interference (for a given configuration of applied stress, crack size, wedge geometry and wedge location).

3

SOLUTION TO PROBLEM A

As indicated in Chapter 2, problem A is that of a line crack subjected to remote biaxial stress and crack face interaction loads. A solution for this problem can be constructed by superimposing solutions available from the literature for biaxial stress at infinity [4] and for concentrated loads acting on the crack face [5]. In this chapter, these solutions are presented as complex stress functions, from which expressions for displacement of the crack faces are then developed. Following this, the relative displacements will be determined and combined to form the load-displacement relationship for problem A.

Complex Variable Formulation

Before the previously mentioned solutions are presented, the complex variable formulation for the equations of two-dimensional elasticity is introduced. Although two separate formulations are presented below, either set of equations could be used for both solutions. However, the solutions will not be combined until displacements have been determined, and so their stress functions need not be reconciled. Thus, use of a single set of equations is not required.

Following the notation from the cited works, we will use

$$2\mu D = \kappa\,\Omega(z) - z\,\overline{\Omega'(z)} - \overline{\omega(z)} \tag{3.1}$$

$$\sigma_{XX} + \sigma_{YY} = 2\left\{\,\Omega'(z) + \overline{\Omega'(z)}\,\right\} \tag{3.2}$$

$$\sigma_{YY} - \sigma_{XX} + 2i\tau_{XY} = -2\left\{\,z\,\overline{\Omega''(z)} + \overline{\omega'(z)}\,\right\} \tag{3.3}$$

for biaxial stress at infinity and

$$2\mu D = \kappa \int_0^z \phi(z)\, dz - \int_0^{\bar{z}} \Omega(\bar{z})\, d\bar{z} - (z - \bar{z})\, \overline{\phi(z)} \tag{3.4}$$

$$\sigma_{XX} + \sigma_{YY} = 2\left\{ \phi(z) + \overline{\phi(z)} \right\} \tag{3.5}$$

$$\sigma_{YY} - \sigma_{XX} + 2i\tau_{XY} = 2\left\{ (\bar{z} - z)\, \phi'(z) - \phi(z) + \overline{\Omega(z)} \right\} \tag{3.6}$$

for concentrated loads on the crack faces, where

$z = x + iy$

$D = u + iv$

$$\kappa = \begin{cases} 3 - 4\nu & \text{plane strain} \\ \dfrac{3 - 4\nu}{1 + \nu} & \text{generalized plane stress} \end{cases}$$

u, v = x and y components, respectively, of displacement

μ = shear modulus

ν = Poisson's ratio

$\Omega(z)$, $\omega(z)$ = complex stress functions in (3.1-3)

$\phi(z)$, $\Omega(z)$ = complex stress functions in (3.4-6)

Note that $\Omega(z)$ does not represent the same function in both sets of equations. With the subscript *BS* (biaxial stress) used to identify stress functions from (3.1-3) and the subscript *CL* (concentrated loads) used to identify those from (3.4-6), the following relationships are supplied for reference.

$$\phi_{CL}(z) = \Omega'_{BS}(z)$$

$$\Omega_{CL}(z) = \overline{\Omega'_{BS}(z)} + \bar{z}\,\overline{\Omega''_{BS}(z)} + \overline{\omega'_{BS}(z)}$$

Biaxial Stress at Infinity

The problem of a plate containing an unstressed central crack and subjected to known stresses at infinity is itself equivalent to the summation of two problems. The first is an uncracked plate with the known stresses at infinity. The second is a cracked plate with a stress distribution, equal in magnitude but opposite in sign to that in the first problem, acting only on the faces of the crack. For the first problem, the complex stress functions are [4]

$$\Omega(z) = \frac{1}{4}(T_1 + T_2)\,z \tag{3.7}$$

$$\omega(z) = -\frac{1}{2}(T_1 - T_2 - 2iS)\,z \tag{3.8}$$

where

$$\sigma_{XX} = T_1$$

$$\sigma_{YY} = T_2$$

$$\tau_{XY} = S$$

at infinity. In the second problem,with the crack positioned on the x-axis and lying along the interval $(-a, a)$, the complex stress functions are [4]

$$\Omega(z) = -\frac{1}{2}(T_2 - iS)\left[\, z - \sqrt{z^2 - a^2}\,\right] \tag{3.9}$$

$$\Theta(z) = C \tag{3.10}$$

where

a = crack half-length

C = constant of integration

and $\Omega(z)$, $\omega(z)$, and $\Theta(z)$ are related by the expression

$$\Theta(z) = \Omega(z) - z\,\overline{\Omega'(\bar{z})} - \overline{\omega(\bar{z})} \tag{3.11}$$

Substitution of the stress functions from the first problem, equations (3.7-8), into (3.1) gives the displacement field

$$2\mu D = \left[\frac{1}{4}(\kappa-1)(T_1 + T_2) + \frac{1}{2}(T_1 - T_2) - iS\right] z \tag{3.12}$$

To obtain the displacements for the second problem, (3.11) must be solved for $\omega(z)$. With this expression and (3.9-10), (3.1) yields

$$2\mu D = -\frac{1}{2}(T_2 - iS)\left\{\kappa\left[z - \sqrt{z^2 - a^2}\right] - \left[\bar{z} - \sqrt{\bar{z}^2 - a^2}\right]\right\}$$
$$- \frac{1}{2}(T_2 + iS)\left[1 - \frac{\bar{z}}{\sqrt{\bar{z}^2 - a^2}}\right] + C \tag{3.13}$$

Since C corresponds to a rigid displacement of the entire body, it can be set to zero. Summation of (3.12-13) then gives

$$2\mu D = \left[\frac{1}{4}(\kappa-1)(T_1 + T_2) + \frac{1}{2}(T_1 - T_2) - iS\right] z$$
$$- \frac{1}{2}(T_2 - iS)\left\{\kappa\left[z - \sqrt{z^2 - a^2}\right] - \left[\bar{z} - \sqrt{\bar{z}^2 - a^2}\right]\right\}$$
$$- \frac{1}{2}(T_2 + iS)\left[1 - \frac{\bar{z}}{\sqrt{\bar{z}^2 - a^2}}\right] \tag{3.14}$$

which is the general displacement field for a cracked plate under biaxial stress.

Because the required displacements are those of the crack face, (3.14) must be evaluated for $y = 0$. As y approaches zero, the terms in (3.14) which involve only z or $\bar{z}$ will simply reduce to x, thereby eliminating the last term altogether. However, evaluation of the terms $\sqrt{z^2 - a^2}$ and $\sqrt{\bar{z}^2 - a^2}$ is more complicated. Paying strict attention to the limiting values obtained when approaching the crack from above and below, we find

that as $y \to 0$,

$$\sqrt{z^2 - a^2} \to \pm i\sqrt{a^2 - x^2} \tag{3.15}$$

$$\sqrt{\bar{z}^2 - a^2} \to \mp i\sqrt{a^2 - x^2} \tag{3.16}$$

and (3.14) becomes

$$2\mu D = \left[\frac{1}{4}(\kappa-1)(T_1 + T_2) + \frac{1}{2}(T_1 - T_2) - iS\right] x$$

$$- \frac{1}{2}(T_2 - iS)\left[(\kappa-1)x \mp i(\kappa+1)\sqrt{a^2 - x^2}\right] \tag{3.17}$$

As a final step, we expand our formulation to accommodate arbitrarily oriented biaxial stress. This is accomplished using the transformation law for components of a second order tensor [6], which gives

$$\sigma_{XX} = \sigma_1 \sin^2\beta + \sigma_2 \cos^2\beta \tag{3.18}$$

$$\sigma_{YY} = \sigma_1 \cos^2\beta + \sigma_2 \sin^2\beta \tag{3.19}$$

$$\tau_{XY} = (\sigma_1 - \sigma_2) \sin\beta \cos\beta \tag{3.20}$$

where σ_1, σ_2 and β are shown in Figure 2.1. Substituting (3.18-20) for the appropriate values in (3.17), we obtain

$$2\mu D = \left[\frac{1}{4}(\kappa-1)(\sigma_1 + \sigma_2) - \frac{1}{2}(\sigma_1 - \sigma_2)\cos 2\beta\right.$$

$$\left. - i(\sigma_1 - \sigma_2)\cos\beta \sin\beta\right] x - \frac{1}{2}\left\{\left[(\sigma_1 \cos^2\beta - \sigma_2 \sin^2\beta)\right.\right.$$

$$\left.\left. - i(\sigma_1 - \sigma_2)\cos\beta \sin\beta\right]\left[(\kappa-1)x \mp i(\kappa+1)\sqrt{a^2 - x^2}\right]\right\} \tag{3.21}$$

Concentrated Loads on the Crack Faces

The solution for the problem of concentrated loads acting on the crack faces is found by considering the general problem of a cracked plate with zero stress at infinity and subjected to concentrated loads as illustrated in Figure 3.1. For this problem, the complex stress functions are [5]

$$\phi(z) = \frac{-S}{z - z_0} + \phi_0(z) \tag{3.22}$$

$$\Omega(z) = \frac{\kappa S}{z - \overline{z_0}} + \frac{\overline{S}(\overline{z_0} - z_0) + im}{(z - \overline{z_0})^2} + \phi_0(z) \tag{3.23}$$

where

$$S = \frac{Q + iR}{2\pi(\kappa + 1)}$$

$$m = \frac{M}{2\pi}$$

z_0 = location on the plate at which the concentrated loads act, $z_0 = x_0 + iy_0$

Q, R = x and y components, respectively, of a concentrated force

M = moment

and κ is the same as for (3.1-6). In addition,

$$\phi_0(z) = \frac{1}{2\pi\sqrt{z^2 - a^2}} \left\{ \frac{S}{z - z_0}\left[I(z) - I(z_0) \right] - \frac{\kappa S}{z - \overline{z_0}}\left[I(z) - I(\overline{z_0}) \right] \right.$$

$$\left. - \left[\overline{S}(\overline{z_0} - z_0) + im \right] \left[\frac{I(z) - I(\overline{z_0})}{(z - \overline{z_0})^2} - \frac{J(\overline{z_0})}{z - z_0} \right] \right\} \tag{3.24}$$

where

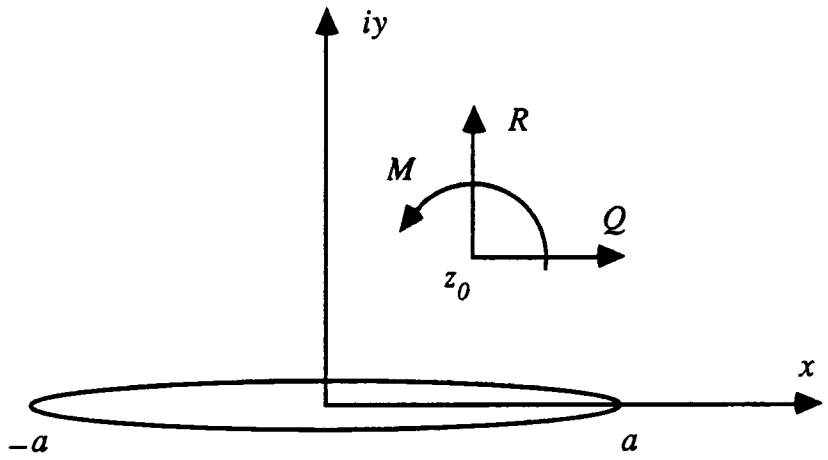


Figure 3.1. Infinite Plate With a Central Crack. Orientation of concentrated loads acting at an arbitrary location, z_0, in a cracked plate with zero stress at infinity.

$$I(z) = \int_{-a}^{a} \frac{\sqrt{a^2 - t^2}}{t - a}\, dt = \pi\sqrt{z^2 - a^2} - \pi z \tag{3.25}$$

$$J(z) = \int_{-a}^{a} \frac{\sqrt{a^2 - t^2}}{(t - a)^2}\, dt = \frac{\pi z}{\sqrt{z^2 - a^2}} - \pi \tag{3.26}$$

for all z except along the crack.

In the particular case where the concentrated loads act directly on the crack faces, (3.22-26) must be evaluated for $y_0 = 0$. Accordingly, (3.25-26) give

$$I(z_0) \rightarrow I^{\pm}(x_0) = \pm\pi\sqrt{x_0^2 - a^2} - \pi x_0$$

$$I(\overline{z_0}) \rightarrow I^{\mp}(x_0) = \mp\pi\sqrt{x_0^2 - a^2} - \pi x_0$$

$$J(z_0) \rightarrow J^{\pm}(x_0) = \pm\frac{\pi x_0}{\sqrt{x_0^2 - a^2}} - \pi$$

and (3.24) becomes

$$\phi_0^{\pm}(z) = \frac{-1}{2(z - x_0)} \left\{ S(\kappa - 1)\left[1 - \frac{(z - x_0)}{\sqrt{z^2 - a^2}}\right] + \frac{im}{z - x_0} \right.$$

$$\left. \pm \left[S(k + 1) + \frac{im}{z - x_0} \right] \frac{\sqrt{x_0^2 - a^2}}{\sqrt{z^2 - a^2}} \pm im\left[\frac{x_0}{\sqrt{(x_0^2 - a^2)(z^2 - a^2)}}\right] \right\} \tag{3.27}$$

where the superscripts $+$ and $-$ indicate loads acting on the upper and lower crack faces respectively. If we now consider (3.22-23), substitution of (3.27) yields

$$\phi(z) = \frac{-S}{z - x_0} + \phi_0^{\pm}(z) \tag{3.28}$$

$$\Omega(z) = \frac{\kappa S}{z - x_0} + \frac{im}{(z - x_0)^2} + \phi_0^{\pm}(z) \tag{3.29}$$

which is the general solution for concentrated loads acting directly on the crack faces. The values of S and m in these equations are determined by the orientation of the applied loads.

For our problem, crack-face interaction is composed of opposing shear and normal forces and additive moments, with the corresponding components being equal in magnitude. This situation is aptly described by Figure 2.5. Combining the complex stress functions for the two load groups, we have

$$\phi(z) = \frac{-S(\kappa+1)}{z - b}\frac{\sqrt{a^2 - b^2}}{\sqrt{a^2 - z^2}} - \frac{im}{(z - b)^2} \tag{3.30}$$

$$\Omega(z) = \frac{-S(\kappa+1)}{z - b}\frac{\sqrt{a^2 - b^2}}{\sqrt{a^2 - z^2}} + \frac{im}{(z - b)^2} \tag{3.31}$$

where

$$S = -\left[\frac{Q - iR}{2\pi(\kappa+1)}\right]$$

$$m = -\frac{M}{2\pi}$$

and x_0 is redefined as b. Before displacements can be obtained, however, the integrals in (3.4) must be determined. For (3.30-31), we find

$$\kappa\int_0^z \phi(z)\,dz = -\kappa\left\{S(\kappa+1)\ln\left[\frac{a^2 - bz + i\sqrt{(a^2 - b^2)(z^2 - a^2)}}{a^2 - bz - i\sqrt{(a^2 - b^2)(z^2 - a^2)}}\right] + \frac{im}{z - b}\right\} \tag{3.32}$$

$$\int_0^{\bar{z}} \Omega(\bar{z})\, d\bar{z} = -\left\{ S(\kappa+1) \ln\left[\frac{a^2 - b\bar{z} + i\sqrt{(a^2 - b^2)(\bar{z}^2 - a^2)}}{a^2 - b\bar{z} - i\sqrt{(a^2 - b^2)(\bar{z}^2 - a^2)}} \right] - \frac{im}{\bar{z} - b} \right\} \tag{3.33}$$

Since we are only interested in displacement of the crack faces, (3.4), and so (3.32-33), must be evaluated for $y = 0$. With (3.15-16), the resulting displacement field is

$$2\mu D = S(\kappa+1)^2 \ln\left[\frac{a^2 - bx \pm \sqrt{(a^2 - b^2)(x^2 - a^2)}}{a^2 - bx \mp \sqrt{(a^2 - b^2)(x^2 - a^2)}} \right] + \frac{im(\kappa+1)}{\bar{x} - b} \tag{3.34}$$

Load-Displacement Relationship

Although the combination of (3.21) and (3.34) will produce the displacement field for problem A, it is only the relative displacements which affect the crack tip stress field. The relative displacements Δu and Δv were defined in Chapter 2 by (2.1-2), respectively. If we first relate S in (3.30-31) to the concentrated load of problem B (see Figure 2.4), these equations give

$$\Delta u = \frac{1}{2\mu}(\kappa+1)(\sigma_1 - \sigma_2)\cos\beta \sin\beta \sqrt{a^2 - x^2} \tag{3.35}$$

$$\Delta v = \frac{1}{2\mu}(\kappa+1)(\sigma_1 \cos^2\beta - \sigma_2 \sin^2\beta)\sqrt{a^2 - x^2} \tag{3.36}$$

for biaxial stress at infinity, equation (3.21), and

$$\Delta u = \frac{-(\kappa+1) P \cos\alpha}{4\pi\mu} \ln\left[\frac{a^2 - bx + \sqrt{(a^2 - b^2)(a^2 - x^2)}}{a^2 - bx - \sqrt{(a^2 - b^2)(a^2 - x^2)}} \right] \tag{3.37}$$

$$\Delta v = \frac{(\kappa+1)\,P \sin\alpha}{4\pi\mu} \ln\left[\frac{a^2 - bx + \sqrt{(a^2 - b^2)(a^2 - x^2)}}{a^2 - bx - \sqrt{(a^2 - b^2)(a^2 - x^2)}}\right] \tag{3.38}$$

for concentrated loads on the crack faces, equation (3.34). From these results and (2.3), the load-displacement relationship for problem A can be written in terms of nondimensional variables as

$$\delta_A^{\,*} = A_1 - A_2 P^* \tag{3.39}$$

where

$$A_1 = (C_1 - C_2 \tan\alpha)\,\sigma^*$$

$$A_2 = C_3(\cos\alpha - \sin\alpha \tan\alpha)$$

$$C_1 = \frac{1}{2}(\kappa+1)(1-\rho)\cos\beta \sin\beta \sqrt{1 - (B + X)^2}$$

$$C_2 = \frac{1}{2}(\kappa+1)(\cos^2\beta - \rho \sin^2\beta)\sqrt{1 - (B + X)^2}$$

$$C_3 = \frac{(\kappa+1)}{4\pi} \ln\left\{\frac{1 - BX + \sqrt{(1 - B^2)\left[1 - (B + X)^2\right]}}{1 - BX - \sqrt{(1 - B^2)\left[1 - (B + X)^2\right]}}\right\}$$

$$X = \frac{h}{a}\tan\alpha$$

$$B = \frac{b}{a}$$

4

SOLUTION TO PROBLEM B

In Chapter 2, problem B was defined as a half-plane with a wedge-shaped bump on the boundary subjected to a concentrated force acting normal to one face of the wedge. Unlike the solution to problem A, no solution to problem B is currently available from the literature. The discussion presented below is based on an original solution yet to be published [7].

Complex Variable Formulation

The solution to problem B is based on the complex variable formulation of the equations of two-dimensional elasticity. However, this solution involves mapping problem B to a simpler geometry, and so requires a slight modification of the equations given in Chapter 3. Following the notation used in (3.1-3), we have for displacements

$$2\mu D = \kappa \Omega(\zeta) - \frac{m(\zeta)}{m'(\zeta)} \overline{\Omega'(\zeta)} - \overline{\omega(\zeta)} \tag{4.1}$$

where

$\zeta = \xi + i\eta$

ξ, η = x and y components, respectively, of the complex variable, ζ, to whose plane problem B is mapped

$\Omega(\zeta), \omega(\zeta)$ = complex stress functions

$m(\zeta)$ = mapping function

and μ, D and κ are the same as in (3.1-6).

Solution Method

First, problem B is mapped to a half-plane using a degenerate Schwartz-Christoffel transformation with only three vertices not at infinity. The mapping function is

$$m(\zeta) = \frac{h}{B(\alpha,1)\cos\alpha} \int_0^{\zeta} \left(\frac{t^2 - 1}{t^2} \right)^{\gamma} dt \tag{4.2}$$

where

$$B(\alpha,1) = \int_0^1 \left(\frac{1 - s^2}{s^2} \right)^{\gamma} ds$$

$$\gamma = \frac{1}{2} - \frac{\alpha}{\pi}$$

and both h and α are shown in Figure 2.4. Next, the complex stress functions are continued analytically across the protions of the boundary on which no resultant force acts. The stress function $\omega(\zeta)$ can then be defined entirely in terms of $\Omega(\zeta)$ and the map. Examination of the normal stress on the boundary, $\eta = 0$, produces a Hilbert problem whose solution is simple. For the problem at hand, this solution gives

$$\Omega(\zeta) = \frac{-iP}{2\pi} e^{-i\pi\gamma} \ln(\zeta - \xi_P) \tag{4.3}$$

$$\omega(\zeta) = -\left[\overline{\Omega(\bar{\zeta})} + \frac{\overline{m(\bar{\zeta})}}{m'(\zeta)} \Omega'(\zeta) \right] \tag{4.3}$$

where P is the contact force and ξ_P is the distance in the ζ-plane which corresponds to r in Figure 2.4. The value of ξ_P is found by iteration using

$$B(\alpha,\xi) = \int_0^{\xi} \left(\frac{1 - s^2}{s^2}\right)^{\gamma} ds \tag{4.5}$$

$$B(\alpha,\xi_P) = \frac{r}{h} \cos\alpha\, B(\alpha,1) \tag{4.6}$$

Load-Displacement Relationship

The displacement field for problem B is determined by substituting (4.3-4) into (4.1). For our purposes, only the x-direction displacements of the points corresponding to points O and P in Figure 2.4 are required. Since these points lie along the y axis, $\zeta = i\,\eta$, and (4.1) yields

$$u = -F(\eta)\,P \tag{4.7}$$

where

$$F(\eta) = \frac{1}{4\pi\mu} \left\{ \frac{2\,A(\alpha,\eta)\,(\xi_P \sin\alpha - \eta\,\cos\alpha)}{(\xi_P{}^2 + \eta^2)\left(\frac{1 + \eta^2}{\eta^2}\right)^{\gamma}} \right\}$$

$$\left\{ -\sin\alpha\,(\kappa - 1)\left[\pi - \tan^{-1}\left(\frac{\eta}{\xi_P}\right)\right] - \frac{1}{2}\cos\alpha\,(k+1)\ln(\xi_P{}^2 + \eta^2) \right\}$$

$$A(\alpha,\eta) = \int_0^{\eta} \left(\frac{1 + s^2}{s^2}\right)^{\gamma} ds$$

From this result and (2.5), the load displacement relationship for Problem B can be written in terms of nondimensional variables as

$$\delta_B^* = 2\left[F(\eta_O) - F(\eta_P)\right]P^* \tag{4.8}$$

where the values of η_O and η_P are found by iteration from

$$A(\alpha,\eta_O) = \cos\alpha\, B(\alpha,1) \tag{4.9}$$

$$A(\alpha,\eta_P) = \frac{r}{h}\cos^2\alpha\, B(\alpha,1) \tag{4.10}$$

5

FORMULATION FOR MULTIPLE INTERFERENCE SITES

A direct extension of our analysis for a crack with a single interference site is that for a crack with multiple interference sites. With the use of superposition, the formulation for multiple sites can be easily obtained from the single site solution. (The use of superposition is consistent with the earlier uses of linear elastic theory and the assumption of brittle fracture.) In this chapter, the topics discussed in Chapter 2 will be re-examined for the multiple site problem. However, only those equations which must be changed to accomodate multiple sites will be documented in this discussion.

To investigate the problem of multiple interference sites, the changes required in the interference model are essentially modifications of problem A. For each additional site, a solution for concentrated loads acting on the crack faces is combined by superposition with the original problem A solution for a single interference site. Figure 2.2 would then show concentrated loads acting at several locations. Iteration between the solutions for the "combined" problem A and problem B is still used to find the contact forces. However, P^* is now a vector of contact forces identified as

$$P_i^* = \frac{P}{\mu a} \qquad i = 1, 2, \ldots, n \tag{5.1}$$

where P is the contact force at site i. Consequently, problem B must be utilized for each interference site to obtain compatibility. In form, the compatibility condition, equation (2.7), remains unchanged when multiple sites are considered. But, since more than one

contact force must be found, the correct values of P_i^* are those which satisfy (2.7) simultaneously at all sites.

While the load-displacement relationship for problem B does not change when multiple sites are considered, the relationship for problem A must accomodate the superposition of several interference sites. Hence, we have

$$\delta_{A_i}^* = A_{1_i} - \sum_{j=1}^{n} A_{2_{ij}} P_j^* \qquad i = 1, 2, \ldots n \tag{5.2}$$

where

$$A_{1_i} = (C_{1_i} - C_{2_i} \tan \alpha)\, \sigma^*$$

$$A_{2_{ij}} = C_{3_{ij}} (\cos \alpha + \sin \alpha \tan \alpha)$$

$$C_{1_i} = \frac{1}{2}(\kappa + 1)(1 - \rho) \cos \beta \sin \beta \sqrt{1 - (B_i + X)^2}$$

$$C_{2_i} = \frac{1}{2}(\kappa + 1)(\cos^2 \beta - \rho \sin^2 \beta) \sqrt{1 - (B_i + X)^2}$$

$$C_{3_{ij}} = \frac{(\kappa + 1)}{4\pi} \ln \left\{ \frac{1 - B_j(B_i + X) + \sqrt{(1 - B_j^2)\left[1 - (B_i + X)^2\right]}}{1 - B_j(B_i + X) - \sqrt{(1 - B_j^2)\left[1 - (B_i + X)^2\right]}} \right\}$$

$$X = \frac{h}{a} \tan \alpha$$

$$B_i = \frac{b_i}{a}$$

In this formulation, the wedge geometry (height and half-angle) of every interference site is identical. If the geometry of individual sites varied within a given crack configuration, contact of the wedges at each interference site would have to be continuously verified. In addition, it is unclear whether the iteration procedure used for this investigation would converge for such a problem .

Although the conditions for interference are not changed by considering multiple interference sites, the restrictions they impose must still be satisfied. For the limits on the contact forces though, equation (2.16), a change in the upper limit is made. This inequality becomes

$$0 < P_j^* < \frac{A_{1_i}}{A_{2_{ij}}} \qquad i = j \tag{5.3}$$

which sets the upper limit on the contact force at each site as that which would be provided by a rigid wedge at that location if no other interference sites were present. Although (5.3) is valid, the upper limit clearly exceeds the maximum value that the contact forces can attain and still meet the compatibility condition, equation (2.7), for multiple sites. Nevertheless, to obtain a more accurate upper limit from (5.2), the values of the contact forces would have to be known, or at least estimated.

While the iteration procedure remains basically the same for the multiple site problem, it must be repeated for each interference site. In addition, while one iteration sequence is sufficient to produce the single site solution, the same is not true for multiple sites. Not only must the current value of the contact force be checked for convergence, but all values of P_i^* must be compared to those obtained from the previous iteration sequence. This requires a minimum of two passes through the iteration procedure for the multiple site solution to converge. Furthermore, convergence is not assumed to occur until the difference between the values of the contact load in the current and previous iteration sequences is suitably small for all sites.

Just as for the single site solution, the Griffith fracture criterion can be used to find R (the required fracture toughness ratio) when multiple sites are considered. Since the presence of the contact force requires Δ_I and Δ_{II} to be calculated for a single interference

site, increasing the number of sites will affect only these terms. Recalling (2.17-18), we now have

$$\Delta_I = \frac{\sin \alpha}{\pi D_I} \sum_{i=1}^{n} \sqrt{\frac{1 + B_i}{1 - B_i}} \frac{P_i^*}{\sigma^*} \tag{5.4}$$

$$\Delta_{II} = \frac{\cos \alpha}{\pi D_{II}} \sum_{i=1}^{n} \sqrt{\frac{1 + B_i}{1 - B_i}} \frac{P_i^*}{\sigma^*} \tag{5.5}$$

where D_I and D_{II} are defined in (2.17-18).

6

RESULTS AND CONCLUSIONS

The following results are shown for stress case I (biaxial tension), which is identified in Table 2.2 and for which the middle column of Table 2.1 applies.

Results for a Single Interference Site

For a single interference site, Figures 6.1 through 6.6 illustrate the influence of various parameters on the required fracture toughness ratio, R. As identified in (2.22), R is the ratio of the fracture toughness required to prevent unstable crack propagation when interference is absent to that required when interference is present. The abscissa in these figures is the applied stress, σ^*, which is defined in (2.8). The range of σ^* is set by (2.12). In the following figures, values of σ^* which correspond to an initial crack opening displacement of from 0.05 to 0.95 times the wedge height, h, are used.

In Figure 6.1, the dependence of R on the wedge half-angle, α, is illustrated. For increasing values of σ^*, the location of the contact load moves toward the apex of the wedge. As a result, the wedge becomes more flexible and the amount of relative shear displacement for a given contact force increases. Correspondingly, the curves shown have negative slopes, with the drop-off being more pronounced for narrow wedges. Narrow wedges have steeper sides, and so present more of a barrrier to relative shear displacement. This is evidenced by the extreme effect seen for wedges whose half-angles lie in the 5 to 10 degree range. With broader wedges, the effect of interference decreases since, for a

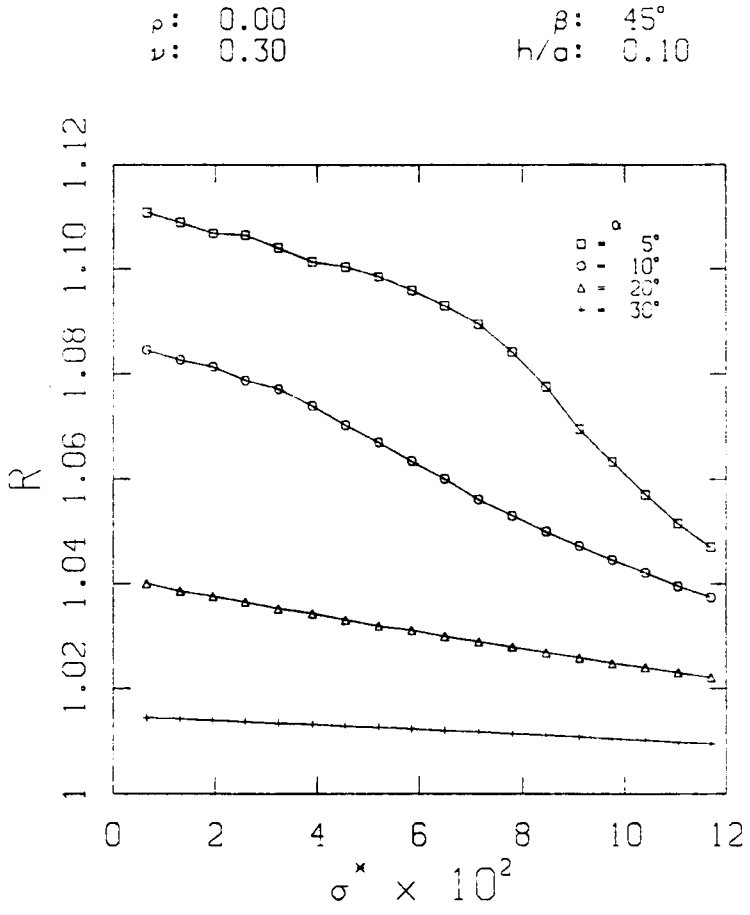


Figure 6.1. Dependence of the Required Fracture Toughness Ratio on the Wedge Half-Angle, α. The interference site is located at the center of the crack. From (2.10), Table 2.1, and the value of ρ and β, above, interference occurs as long as $\alpha < \beta$. Narrow wedges present more of a barrier to relative shear displacement and so the influence of interference increases and α is reduced.

given amount of crack opening, more relative shear displacement must occur to bring the wedges into contact .

Figure 6.2 illustrates the dependence of R on the stress orientation angle, β. Again, the influence of this parameter on the required fracture stress can be considerable. As the value of β increases, the crack is opened less, and so the wedges become more of a barrier to relative shear displacement. Thus, the influence of interference increases. It is physically reasonable to expect that this trend peaks for some value of β and that no interference will occur for $\beta = 90^o$. However, the value at which this occurs has yet to be determined.

The dependence of R on the biaxial stress ratio, ρ, is illustrated in Figure 6.3. The effect of σ_2 is to produce relative shear displacement opposite to that produced by σ_1. Consequently, as the ratio σ_2 of to σ_1 increases, the amount of relative shear displacement which the wedges act to prevent, and so the effect of interference, decreases. In addition, the presence of σ_2 results in more initial crack opening displacement. Hence, the range of applied stress for which interference will occur is also reduced as biaxiality increases.

As shown in Figure 6.4, the variation of Poisson's ratio within physically realistic limits has virtually no effect on R.

The dependence of R on the size of the wedge is illustrated in Figure 6.5. For a given wedge, one whose height is greater will be stiffer and more opening will be required to produce the same amount of bending. Therefore, as wedge height increases, the effect on R and the range of applied stress which produces interference increases. It is clear that if the wedges are too large relative to the crack size then replacing them with concentrated loads in problem A is not appropriate.

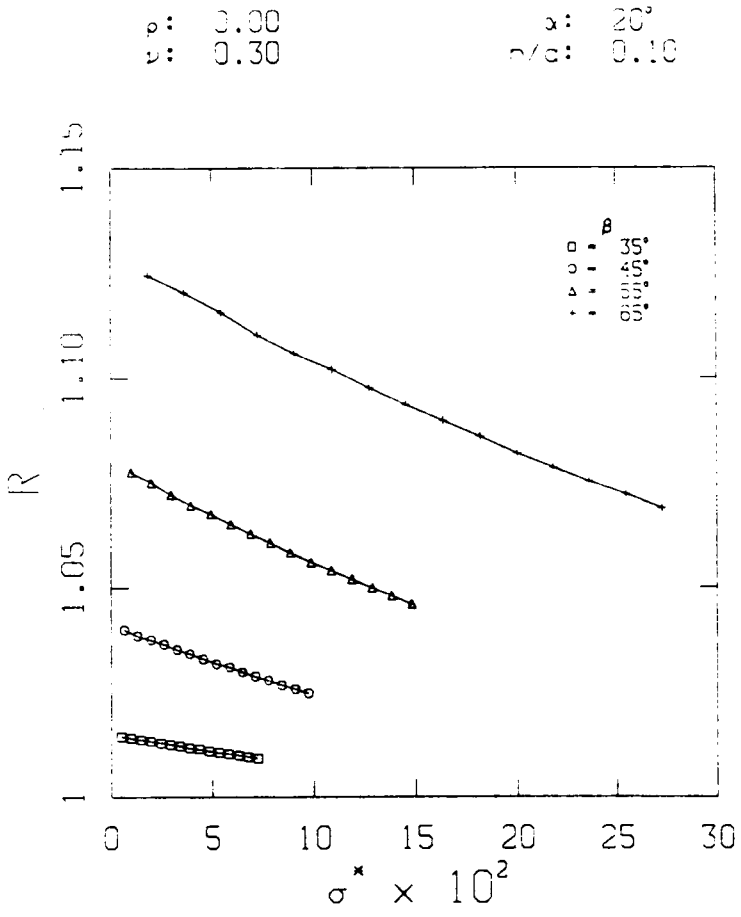


Figure 6.2. Dependence of the Required Fracture Toughness Ratio on the Stress Orientation Angle, β. The interference site is located at the center of the crack. Since less crack opening is produced as β increases, the contact load acts lower on the faces of the wedges. This causes the wedges to become more of a barrier to relative shear displacement and increases the influence of interference.

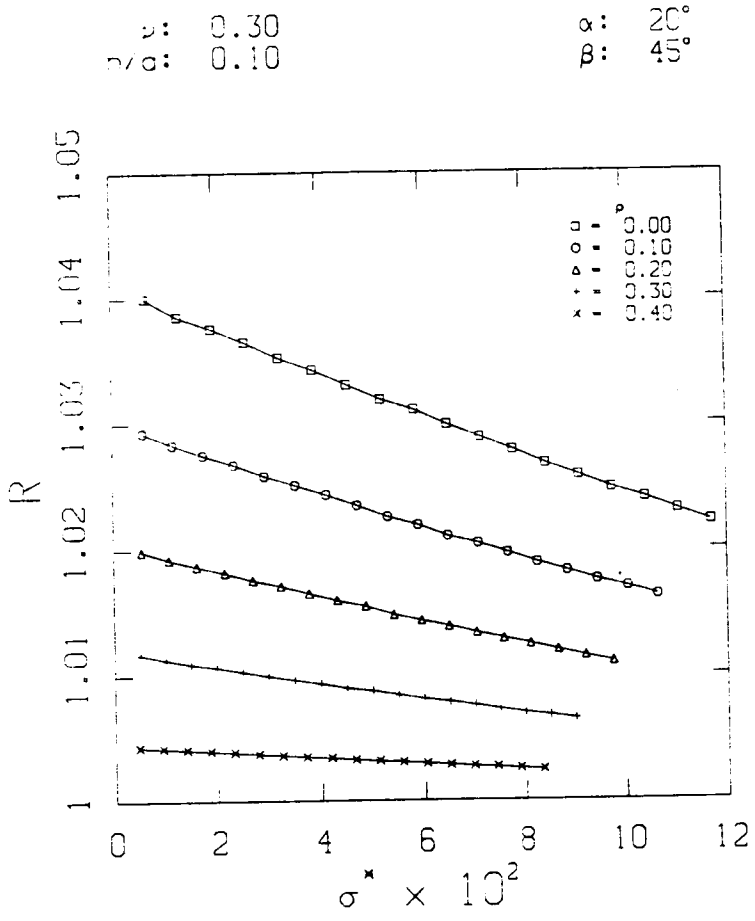


Figure 6.3. Dependence of the Required Fracture Toughness Ratio on the Biaxial Stress Ratio, ρ. The interference site is located at the center of the crack. As σ_2 increases, more opening and less relative shear displacment occurs. Thus, the influence of interference is reduced.

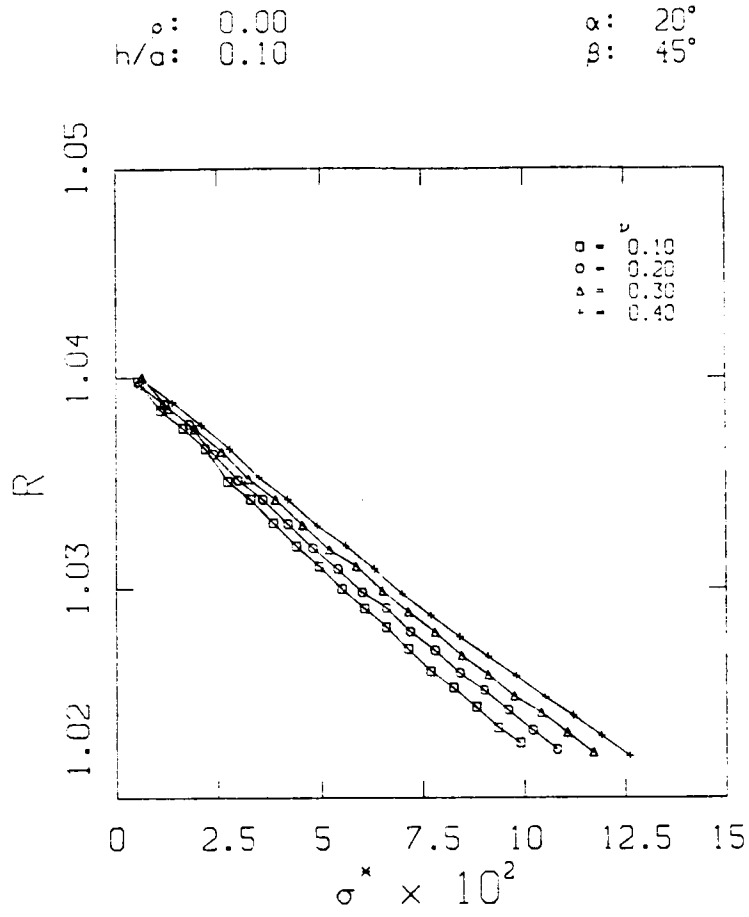


Figure 6.4. Dependence of the Required Fracture Toughness Ratio on Poisson's Ratio, *v*. The interference site is located at the center of the crack. The influence of interference is virtually unchanged by variation of Poisson's ratio within physically realistic limits.

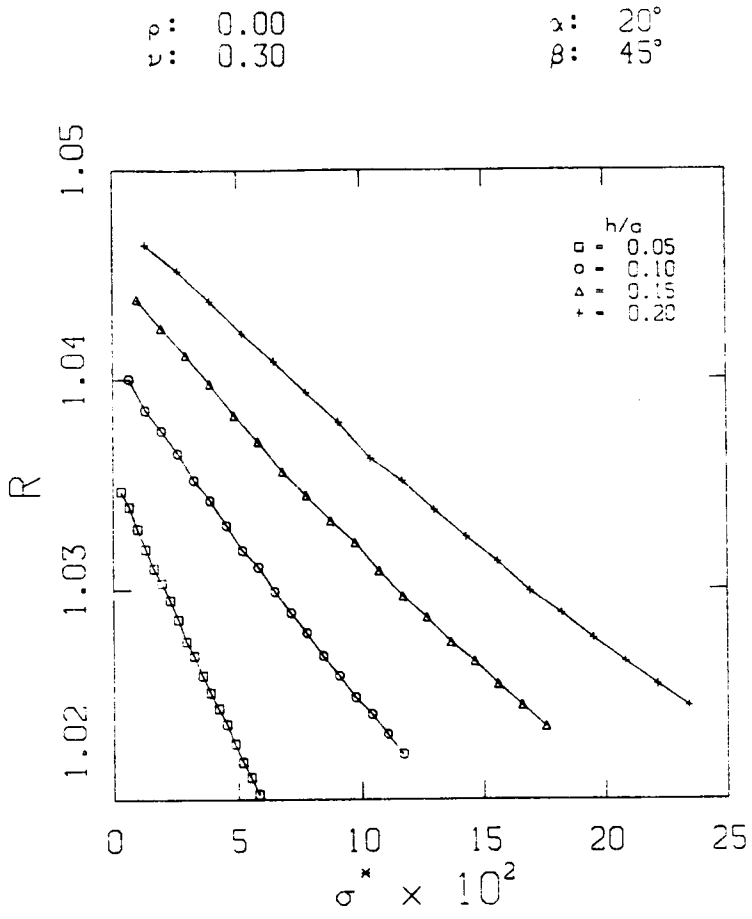


Figure 6.5. Dependence of the Required Fracture Toughness Ratio on the Wedge Height. The interference site is located at the center of the crack. The influence of interference is greater for larger wedges since a taller wedge will be stiffer for a given amount of crack opening and provide more resistance to relative shear displacement.

In Figure 6.6, the dependence of R on the location of the interference site is illustrated. As the interference site approaches the crack tip, its effect on R increases. This is to be expected since a wedge closer to the crack tip will have more influence on the crack tip stress field.

Results for Multiple Interference Sites

From the results shown in Figures 6.1 through 6.6, it is evident that the influence of protrusion interference on the fracture toughness required to prevent unstable crack propagation for a single interference site is small, but can be substantial under certain conditions. Since a real crack with rough faces would not have only one interference site, the problem of multiple interference sites should be investigated.

When multiple interference sites are present, it is not always clear which crack tip, $x = a$ or $x = -a$, is more affected by interference. However, the following results are obtained for site configurations which are symmetric about $x = 0$, and equally spaced between the crack tips. Thus, the influence of interference should be almost the same at both crack tips.

The influence of multiple interference sites on the required fracture toughness ratio, R, is illustrated in Figure 6.7. It is not suprising that an increase in the number of sites causes an increase in R. However, this increase is not linear because additional crack opening results as more sites are included. In Figure 6.8, this effect is illustrated for site configurations which are symmetric about $x = 0$, and equally spaced within the interval $\left(-\frac{a}{2}, \frac{a}{2}\right)$. As shown, the influence of multiple sites appears to approach some limit as the number of sites is increased. For the configuration used to obtain these results, this limit

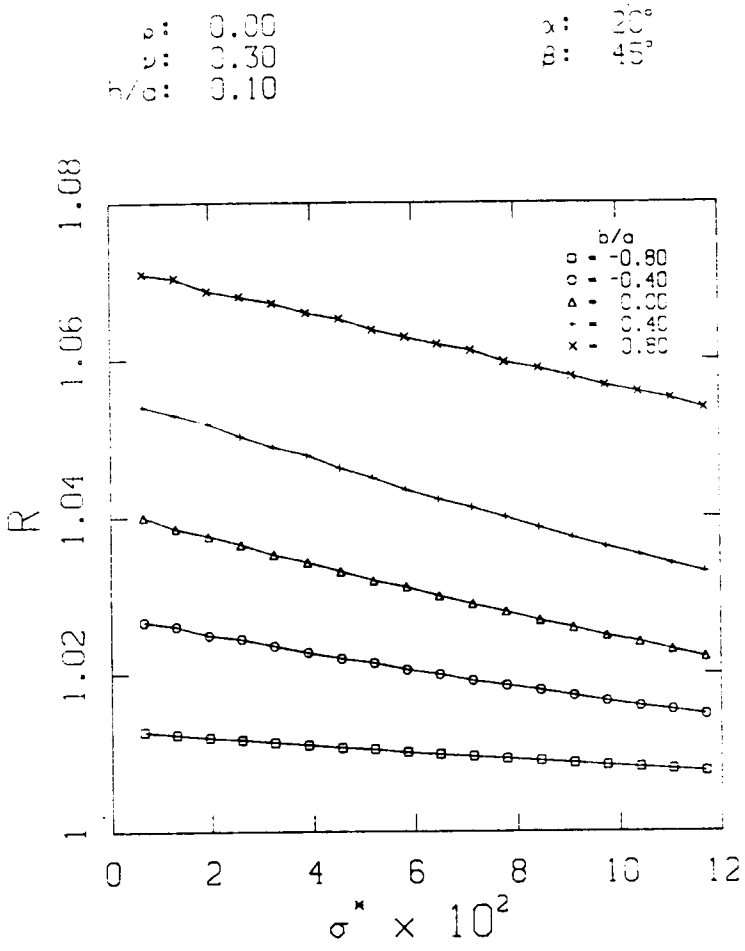


Figure 6.6. Dependence of the Required Fracture Toughness Ratio on the Location of the Interference Site. Interference sites near a particular crack tip have more effect on the stress field at that crack tip. Consequently, as the interference site is placed closer to the crack tip, the influence of interference increases.

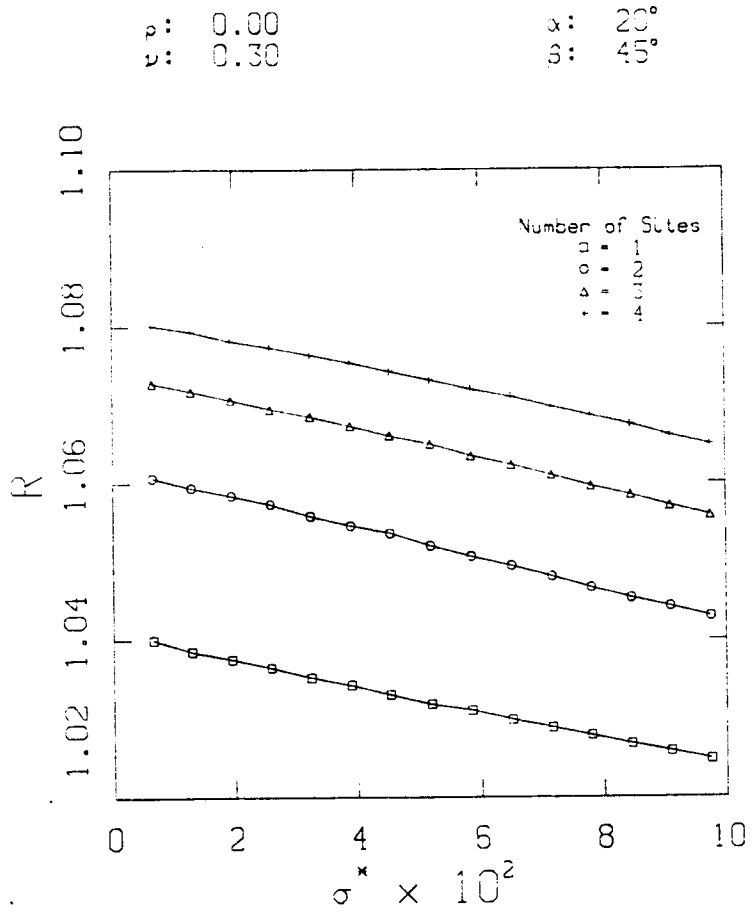


Figure 6.7. Dependence of the Required Fracture Toughness Ratio on the Number of Interference Sites. As the number of sites is increased, less relative shear displacement can occur for a given amount of applied stress, and so the influence of interference increases.

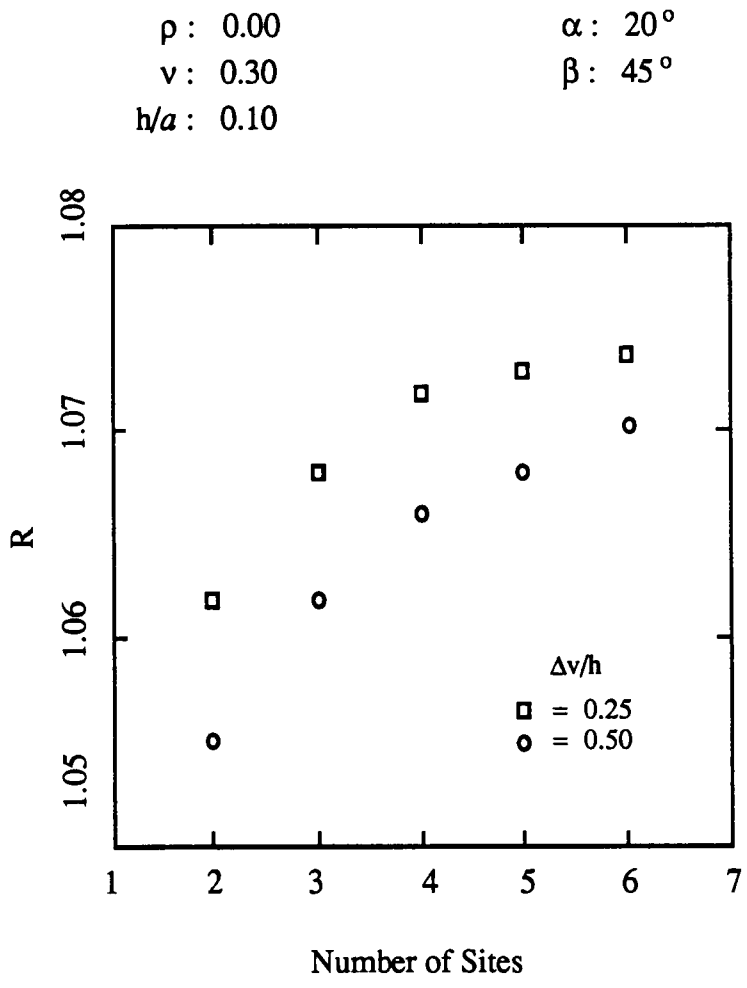


Figure 6.8. Illustration of the Required Fracture Toughness Ratio Approaching a Limit Asymptotically as the Number of Interference Sites is Increased. This effect results from the additional opening produced when more sites are included.

should correspond to the effects produced by two cracks, each with a crack length of $\frac{a}{2}$, separated by a distance of a.

Conclusions

The results presented above are obtained for nondimensional variables and so cannot be directly related to a particular material. In addition, while the influence of the various parameters is examined for the entire range of σ^*, it is unclear how much of this range will be valid for real materials. Since no one fracture criterion has been identified as superior for examining mixed-mode fracture, the influence of interference illustrated by these results could be quite different for another criterion. However, if the results of this investigation are indicative of the trends resulting from protrusion interference, the following conclusions would be in order.

1. The influence of a single interference site is of small importance, except under certain special conditions which cannot be guaranteed to exist for actual cracks.

2. While the influence of multiple interference sites increases monotonically with the number of sites, it appears to approach some limit asymptotically as more sites are included.

LIST OF REFERENCES

LIST OF REFERENCES

[1] H. M. Westergaard, "Bearing Pressures and Cracks," *Journal of Applied Mechanics,* 6(2), 1939, A - 49.

[2] D. Broek, *Elementary Engineering Fracture Mechanics*, Martinus Nijhoff Publishers, 1986.

[3] P. Paris and G. C. Sih, "Stress Analysis of Cracks," *Fracture Toughness Testing and Its Applications, STP 381*, ASTM, 1965, pp. 30 - 81.

[4] A. H. England, *Complex Variable Methods in Elasticity*, Wiley - Interscience, 1971.

[5] F. Erdogan, "On the Stress Distribution in Plates with Collinear Cuts under Arbitrary Loads," *Proceedings of the Fourth U.S. National Congress of Applied Mechanics, Vol. 1*, ed. R. M. Rosenberg, ASME, 1962, pp. 547 - 553.

[6] Y. C. Fung, *A First Course in Continuum Mechanics*, Prentice Hall, Inc., 1969.

[7] J. A. M. Boulet, "Influence of Protrusion Interference on Biaxial Fracture," in preparation.

VITA

John Darrek Offutt was born in Columbus, Georgia, on October 5, 1963. He later moved to Tennessee where he attended elementary school and graduated from McMinn Central High School, Englewood, Tennessee, in June 1982.

In August 1987, he received a Bachelor of Science in Engineering Science from The University of Tennessee, Knoxville. That same fall, he was awarded a fellowship at The Graduate School of the University of Tennessee, Knoxville and began study toward a Master's degree. This degree was awarded in December 1989.